EPJ manuscript No.
(will be inserted by the editor)

Differential cross-section measurement of the ^{12}C(e,e′pp)^{10}Be$_{g.s.}$ reaction

M. Makek[1], P. Achenbach[2], C. Ayerbe Gayoso[2], C. Barbieri[3], J.C. Bernauer[2] [a], R. Böhm[2], D. Bosnar[1], A. Denig[2], M.O. Distler[2], I. Friščić[1a], C. Giusti[4], H. Merkel[2], U. Müller[2], L. Nungesser[2], J. Pochodzalla[2], S. Sanches Majos[2], B.S. Schlimme[2], M. Schwamb[2], and Th. Walcher[2]
(A1 Collaboration)

[1] Department of Physics, Faculty of Science, University of Zagreb, HR-10002 Zagreb, Croatia
[2] Institut für Kernphysik, Johannes Gutenberg-Universität, D-55099 Mainz, Germany
[3] Department of Physics, University of Surrey, Guildford GU2 7XH, United Kingdom
[4] Dipartimento di Fisica, Università degli Studi di Pavia and INFN, Sezione di Pavia, Via A. Bassi 6, I-27100 Pavia, Italy

Received: date / Revised version: date

Abstract. The differential cross section was measured for the ^{12}C(e,e′pp)^{10}Be$_{g.s.}$ reaction at energy and momentum transfers of 163 MeV and 198 MeV/c, respectively. The measurement was performed at the Mainz Microtron by using two high-resolution magnetic spectrometers of the A1 Collaboration and a newly developed silicon detector telescope. The overall resolution of the detector system was sufficient to distinguish the ground state from the first excited state in ^{10}Be. We chose a super-parallel geometry that minimizes the effect of two-body currents and emphasizes the effect of nucleon-nucleon correlations. The obtained differential cross section is compared to the theoretical results of the Pavia reaction code in which different processes leading to two-nucleon knockout are accounted for microscopically. The comparison shows a strong sensitivity to nuclear structure input and the measured cross section is seen to be dominated by the interplay between long- and short-range nucleon-nucleon correlations. Microscopic calculations based on the ab-initio self-consistent Green's function method explain the experiment well.

PACS. 21.30.Fe Forces in hadronic systems and effective interactions – 25.30.Fj Inelastic electron scattering to continuum

1 Introduction

Nuclear correlations play a crucial role in our quest to unveil the structure and dynamics of atomic nuclei. They are generically defined as those features of the nuclear structure that cannot be explained in terms of a pure mean-field (that is, an independent particle model) [1,2]. The understanding of these mechanisms is fundamental to achieve precise microscopic *ab-initio* predictions of nuclear phenomena and, in turn, to advance our knowledge of the nuclear interactions.

Since the analysis of early nucleon-nucleon (NN) scattering data, it has been suggested that phase shifts at large energies require strongly repulsive interactions at short distances (r≤1 fm) [3]. Correspondingly, it has become customary to distinguish between short-range correlations (SRC), that describe the effects of a strongly repulsive core and long-range correlations (LRC), which encode collective excitations and shell-model mixing at lower and medium energies. In addition, one refers to tensor correlations as the effects due to the tensor component of the nuclear interaction. These contribute to both LRC and SRC effects, although some investigations only focus on the short-range physics part of it (see for example Refs. [4,5]). The importance of nuclear correlations was established, for example, in the early (e,e′p) experiments [6–8] from which strong reductions of single particle strength was inferred. While such measurements might have initially been conjectured to be short-range effects, later calculations clearly demonstrated that they must be ascribed almost completely to LRC dynamics [2,9,10]. This is confirmed by (e,e′p) observations at small missing energies an large missing momenta [11,12]. Similarly, several studies have put in evidence that saturation properties of nuclear systems can also be explained without the need of a strong short-range repulsion among nucleons [13–15]. However, a recent experiment on ^{12}C [16] found direct evidence of high-momentum components, which in parallel kinematics could hardly be ascribed to final-state interactions effects [17,18]. More related investigations, aimed at addressing the nature of the correlations, followed during the last decade [19,5,20–22]. In particular, the emission of pn pairs was found stronger than the corresponding pp

[a] *Present address:* MIT-LNS, Cambridge MA, 02139, USA
Correspondence to: bosnar@phy.hr

and nn pairs [5], suggesting a sizeable tensorial interaction at short distances [4].

Electromagnetically induced knock-out of NN pairs has been considered for a long time one of the best tools for investigating the correlations [6,23]. In specific kinematic conditions the dominant mechanism is that the photon, virtual or real, knocks out either nucleon of a correlated pair, via one-body nuclear current. When the other nucleon remains in a highly excited state and possesses a relatively large momentum, it will eventually fly out of the system. Hence, the simultaneous detection of two nucleons in an electromagnetic knock-out process can provide insight into nucleon-nucleon correlations. However, the NN structure at low energy can also contribute to the cross section, as well as competing reaction mechanisms involving two-body processes like meson-exchange currents (MEC) and isobar currents (IC). In addition, final-state interactions (FSI) of each outgoing nucleon with the other nucleons need to be taken into account [24–27]. Therefore, the contributions of these different processes should be well under control in order to extract reliable experimental information regarding two-nucleon correlations. The relative contribution of the above processes depends on the reaction type and kinematics. While NN knock-out induced by a real photon is only sensitive to the transverse part of the nuclear current, virtual photons are sensitive to both transverse and longitudinal components. The longitudinal cross section is dominated by one-body currents and is therefore sensitive to correlations. In contrast, two-body currents are strongest in the transverse cross section and can therefore more suitably be studied with real photons. Different properties can be studied using (e,e′pp) and (e,e′pn) reactions. For the (e,e′pn) reaction a major role is generally expected to be played by tensor correlations. For the (e,e′pp) reaction suitable kinematic conditions can be envisaged where the longitudinal contribution of the one-body current dominates and which are able to emphasize the role of SRC.

Measurements where the states of the residual nucleus can be separated are of particular interest in order to discriminate, in comparison with the results of theoretical models, contributions from one- and two-body currents [25]. Such measurements were performed for the first time at NIKHEF for the reaction ^{16}O(e,e′pp)^{14}C [28–30] and gave clear signatures of SRC for the transition to the ground state of ^{14}C. Similar pilot measurement was later carried out at MAMI for the ^{16}O(e,e′pp)^{14}C [31]. Previous (e,e′pp) measurements performed on ^{12}C were not able to distinguish individual states in the residual nucleus [32–34].

In the present paper we report the results of a measurement of the ^{12}C(e,e′pp)^{10}Be reaction performed at MAMI in super-parallel kinematics, that is sensitive to the one-body emission channel, and partially suppresses other mechanisms capable to produce two protons in the final state. A silicon detector telescope (SDT) for proton detection has been developed [35] and employed along with two high-resolution magnetic spectrometers of the A1 Collaboration [36] that have been used for detecting the scattered electron and the other proton. The overall resolution of the detector system provides a clear identification of states in the residual nucleus. We have extracted the differential cross section for the case when ^{10}Be is left in the ground state and compared it with the theoretical results of the Pavia reaction code.

We will discuss important aspects of the reaction mechanism and of the theoretical approach in Sections 2 and 3, by first describing our approach to microscopic calculations of the (e,e′NN) reaction rates and then applying these to discuss the choice of the kinematics for the present ^{12}C(e,e′pp)^{10}Be measurement. Sec. 4 is devoted to the description of the experiment and data analysis. In Sec. 5 we present the experimental results and compare them to the theoretical results.

2 Theoretical framework

In the usual description of electron scattering, a virtual photon transfers to a nucleus an energy $\omega = E_e - E'_e$ and momentum $\boldsymbol{q} = \boldsymbol{p_e} - \boldsymbol{p'_e}$, where the subscripts e and e' represent the incident and scattered electron, respectively.

In the exclusive (e,e′pp) knockout reaction two protons are ejected from the nucleus and are detected in coincidence with the scattered electron. The energy and momentum of the undetected recoiling nucleus, commonly denoted as missing energy, E_m, and missing momentum, $\boldsymbol{p_m}$, are determined by energy and momentum conservation:

$$E_m = \omega - T_{p1} - T_{p2} - T_r = S_{pp} + E_x, \tag{1}$$

$$\boldsymbol{p_m} = \boldsymbol{q} - \boldsymbol{p_{p1}} - \boldsymbol{p_{p2}}, \tag{2}$$

where T_{p1}, T_{p2}, and T_r are the kinetic energies of the two emitted protons and of the recoil nucleus, respectively; T_r can be determined from $\boldsymbol{p_m}$. The residual nucleus can be left in a variety of states with excitation energy E_x, and S_{pp} is the separation energy for the reaction.

The basic ingredients of a cross section calculation are the transition matrix elements of the nuclear-current operator between initial and final nuclear state. For an exclusive reaction, where the residual nucleus is left in a specific discrete eigenstate $|\Psi_n^{A-2}\rangle$, and under the assumption of a direct knock-out mechanism, the transition matrix elements contain three main ingredients: the nuclear current, the two-nucleon overlap function between the ground state of the target and the final state of the residual nucleus, and the two-nucleon scattering wave function [25,37].

The nuclear current is the sum of a one-body part, which includes the longitudinal charge and the transverse convective and spin currents, and of a two-body part, which for the (e,e′pp) reaction includes only the non-charge-exchange terms of the Δ-isobar current. Details about the treatment of the isobar current can be found in [38–40].

The two-nucleon overlap is given by the matrix element for the removal of two nucleons between the ground state of the target and the state of the residual nucleus,

$$\psi^{(2h)}_{s\,s'}(\mathbf{r},\mathbf{r}') = \langle \Psi_n^{A-2} | c_s(\mathbf{r}) c_{s'}(\mathbf{r}') | \Psi^A_{g.s.} \rangle \ , \tag{3}$$

where $c_s(\mathbf{r})$ is the annihilator operator for a nucleon at position $\mathbf{r}$ and with spin/isospin indices s. This is the quantity that contains information on the target structure and, therefore, the nuclear correlations. When contracted with the nuclear current and the scattering mechanisms of the FSI, it produces the cross section. In the present work we compare two different approximations for $\psi^{(2h)}_{s\,s'}(\mathbf{r},\mathbf{r}')$.

In the first case we model this as two independent protons in the $p_{3/2}$ orbit multiplied by a Jastrow correlation function [37]:

$$\psi^{(2h)}_{s\,s'}(\mathbf{r},\mathbf{r}') = f(|\mathbf{r}-\mathbf{r}'|)\,\mathcal{A}\,\left[\phi^{(p_{3/2})}_{s}(\mathbf{r})\otimes\phi^{(p_{3/2})}_{s'}(\mathbf{r}')\right]_{JT}\,, \tag{4}$$

where the two nucleons are coupled in angular momentum and isospin and $\mathcal{A}$ is a proper antisymmetrization operator. The correlation function is such that $f(r\to+\infty)=1$ but $f(r=0)\ll 1$ [41], so that the two-proton overlap function is quenched at very short distances to force the SRC effects of a repulsive core. This will allow to gauge the possible effects from SRC alone.

The second approach to the two-nucleon overlap is instead obtained from a state-of-the-art microscopic calculation done with the *ab-initio* self-consistent Green's function (SCGF) method [42,10]. In the present case, we extract the one-body spectral function in an analogous way to earlier calculations for ^{16}O [43] and use a Bonn-C realistic nuclear force [44]. This semi-phenomenological realistic interaction is know to give simial SRC effects as the Argonne interaction models [45,46,2].We then follow the approach of Ref. [27] and calculate the two-nucleon overlap in the dressed random phase approximation (DRPA) within a limited model space of 5 oscillator shells. Two-nucleon dynamics beyond this model space is taken into account by calculating defect functions of the Bonn-C potential and adding them to the DRPA result. This includes both SRC effects and a highly sophisticated description of LRC. The microscopic DRPA approach has already been applied for the comparison with data of the ^{16}O(e,e′pn)^{14}N knock-out reaction with satisfactory results [47,48].

The two-nucleon scattering wave function contains the effects of FSI due to the interaction of each one of the two outgoing protons with the residual nucleus, which is described in the model by a phenomenological optical potential obtained through a fit of elastic proton-nucleus scattering data [49], as well as the mutual interaction of the two emitted nucleons (NN-FSI), which is included within the perturbative approach reported in [50–52].

Our microscopic calculations include a complete treatment of centre-of-mass (CM) effects as in [53,54]. In the CM frame the transition operator becomes a two-body operator even in the case of a one-body nuclear current. The role of CM effects was discussed in [53,54] in connection with the problem of the orthogonality between the initial and final nuclear states.

3 Kinematics of the ^{12}C(e,e′pp)^{10}Be reaction

The kinematic conditions for the present ^{12}C(e,e′pp)^{10}Be measurement were selected with the aim to emphasize the effects of correlations and minimize the contribution of other mechanisms due to two-body currents and FSI. If one is interested in detecting possible signature of SRC, pp knock-out is preferable to the emission of a pn pair, where tensor correlations are much more important [27]. In addition, concerning the two-body currents, the pion-in-flight and seagull MEC and the charge-exchange part of the Δ-isobar current contribute only in pn knock-out and are vanishing in the nonrelativistic limit for pp knock-out, where only a part of the Δ-current contributes. The role of the Δ-current depends strongly on the kinematics and it does not contribute significantly below the Δ-excitation energy. Therefore, to minimize the isobar contribution, the energy and momentum transfers were selected well below the Δ resonance position, at ω=163 MeV and $|\boldsymbol{q}|$=198 MeV/c, with E_e=480 MeV, E'_e=317 MeV, and an electron scattering angle (with respect to the electron beam) of Θ'_e=-16.5° (we denote positive angles on the virtual photon scattering side). We chose a super-parallel kinematics, where the two protons are emitted anti-parallel to one another, i.e. where the angles of the ejected protons with respect to the momentum transfer are γ_1=0° and γ_2=180°.

To help the choice of the kinematical setting for this measurement, we performed preliminary calculations of the ^{12}C(e,e′pp)^{10}Be$_{g.s.}$ reaction, for the transition to the 0^+ ground state of ^{10}Be, using the Pavia reaction model [53] described in Sec. 2. From the comparison of numerical predictions in different kinematic conditions it was possible to assess the expected magnitude of the cross sections and the role of SRC, Δ-isobar currents, and FSI. Calculations indicate that in the kinematic conditions selected for the present measurement the contribution of the two-body Δ-current is negligible and the cross section is dominated by the one-body current and therefore by correlations. Concerning FSI, the optical potential gives in general a substantial reduction of the calculated cross section that is due to its absorptive imaginary part. This is a well known effect effect that is always present although it depends on the kinematics and it is usually larger in pp than in pn knock-out. For the particular super-parallel kinematics chosen in this work, such a FSI effect is somewhat weaker but still reduces the cross section by more than one order of magnitude. We have also checked using different optical potentials affect the calculate cross sections by much smaller amounts–between a few percent to at most 30-40%–and it does not sensibly affect the comparison with the measured data. In contrast, the interaction between two nucleons in the final state (NN-FSI) varies for different realisations of super-parallel kinematics. This can be either small or become very large for (e,e′pp) [50–53]. The particular setting we used are super-parallel but the remaining kinematic variables were chosen in such a way to reduce NN-FSI, which turned out to be negligible in this work.

4 Experiment and data analysis

4.1 Experimental set-up and measurement

The measurement was performed at the 100% duty factor electron accelerator Mainz Microtron, MAMI, within the experimental set-up of the A1 Collaboration. The scattered electrons were detected in Spectrometer B, the forward emitted protons in Spectrometer A and the backward emitted protons were detected in the SDT (Figure 1). The ^{12}C target thickness was 43.86 mg/cm^2 and it was

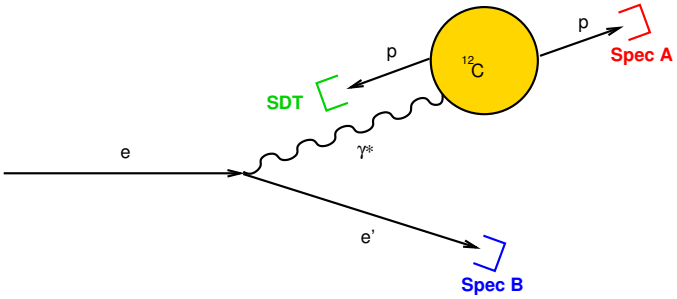

Fig. 1. Schematic diagram of the detector set-up for the $^{12}C(e,e'pp)^{10}Be$ measurement.

rotated 45° ± 3° with respect to the electron beam direction in order to minimize the backward proton energy loss within the target material. The total time of the measurement was 130h, with beam currents 25 μA (121h), 15 μA (5h) and 30 μA (4h), which resulted in an integrated luminosity $\mathcal{L} = (199\pm10)$ fb^{-1}. of ^{10}Be in the $^{12}C(e,e'pp)^{10}Be$ reaction. Spectrometers A and B are high-resolution magnetic spectrometers with solid angles, $\Delta\Omega$, of 28 msr and 5.6 msr, respectively. The momentum acceptance, $\Delta p/p$, of Spectrometer A is 20% and of Spectrometer B is 15%, the momentum resolution, $\delta p/p$, of both spectrometers is better than 10^{-4} and the angular resolution at the target is $\leq$ 3 mrad. The central momentum of Spectrometer A was set to 420 MeV/c and the central angle to 28.0°. The central momentum of Spectrometer B was set to 317 MeV/c and the central angle to -16.5°. In this measurement the total efficiency of detector systems of each of the spectrometers had a standard value of ϵ_{Spect}=0.99 ± 0.01. The Silicon Detector Telescope was at the distance of 8.9 cm from a target subtending the solid angle of 72 msr and providing the angular resolution $\leq$ 1°. It was placed at the central angle of -153.0°. The detected proton kinetic energies were in the range of 25.2 - 40.6 MeV with the mean energy resolution σ_E = 0.47 MeV. The detection efficiency of the SDT for protons was ϵ_{SDT} =0.96 ± 0.01 [35]. It follows that the total detection efficiency of the experimental set-up, consisting of the two spectrometers and the SDT in a triple-coincidence mode, was $\varepsilon = 0.99 \times 0.99 \times 0.96 = 0.94$.

4.2 Data analysis

4.2.1 Identification of e'pp coincidences

Standard procedures and program packages were used for determination of the momenta and identification of the scattered electron detected in spectrometer B and the forward ejected proton detected in spectrometer A [36]. Backward proton identification in the SDT was done by the dE-E method, with dE being the energy measured by the first silicon layer and E being the total energy measured by the subsequent silicon layers. The full momentum four-vector of the proton detected in the SDT was determined as described in [35].

Triple coincidence events were selected on an event-by-event basis by placing requirements on the maximum time differences of the particle detection in each detector pair, t_{A-B}, t_{A-SDT} and t_{B-SDT}. Only two of these time differences were actually independent, so the triple-coincidence requirement was set as $\sqrt{t^2_{A-SDT} + t^2_{B-SDT}} < 2$ ns, which selects more than 99.7 % triple coincidence events. Coincidence time spectra t_{A-B}, t_{A-SDT} and t_{B-SDT} had resolutions (FWHM) 1.2 ns, 1.4 ns and 1.2 ns, respectively.

4.2.2 Background subtraction

The applied coincidence requirement selects all triple coincidence events. However, this sample contains a contribution of the background due to accidental triple coincidences. These can be: (a) A-B (true coincidence) + SDT (accidental), (b) A-SDT (true coincidence) + B (accidental), (c) B-SDT (true coincidence) + A (accidental) and (d) A (accidental)+ B (accidental) + SDT (accidental). The backgrounds are statistically subtracted according to:

$$N = N_{A-B-SDT} - (N_a + N_b + N_c + N_d) + 3N_d \quad (5)$$

where N is the number of the true coincidences, $N_{A-B-SDT}$ is the number of events obtained after making the triple-coincidence cut and $N_{a,b,c,d}$ are the contributions of the coresponding background events. The last term in equation (5) accounts for the fact that the completely accidental background, type (d), is implicitly present in types (a), (b) and (c), however it should be subtracted only once. The background contributions were determined by making the corresponding requirements in the $t_{A-SDT} - t_{B-SDT}$ plane (Figure 2). E.g. the events corresponding to type (b) background were determined by requiring $|t_{A-SDT}| < 2$ ns and 5 ns $< |t_{B-SDT}| <$ 15 ns. The number of these events was then normalized to the area subtended by the triple-coincidence requirement, $\sqrt{t^2_{A-SDT} + t^2_{B-SDT}} < 2$ ns.

4.2.3 ^{10}Be excitation spectrum

After reconstructing the four-momenta of the scattered electron and both protons and selecting the triple coincidence events, the excitation energy of the recoiling nucleus, E$_x$(^{10}Be), was calculated according to:

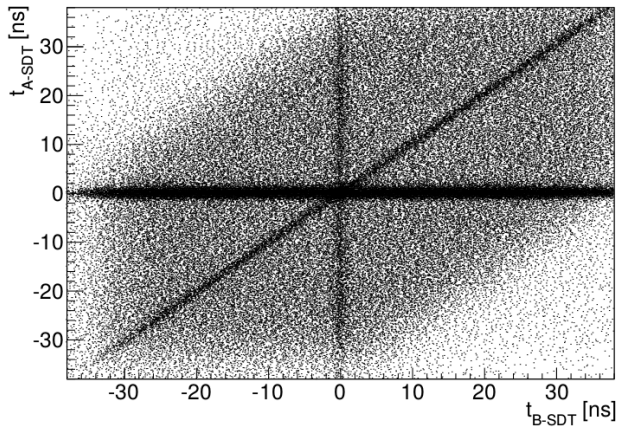

Fig. 2. Coincidence time t_{A-SDT} vs. t_{B-SDT}. The diagonal, the horizontal and the vertical lines correspond to type (a), (b), (c) backgrounds (see text), respectively. The areas between the lines correspond to type (d) background. The crossing of the three lines corresponds to the triple coincidences.

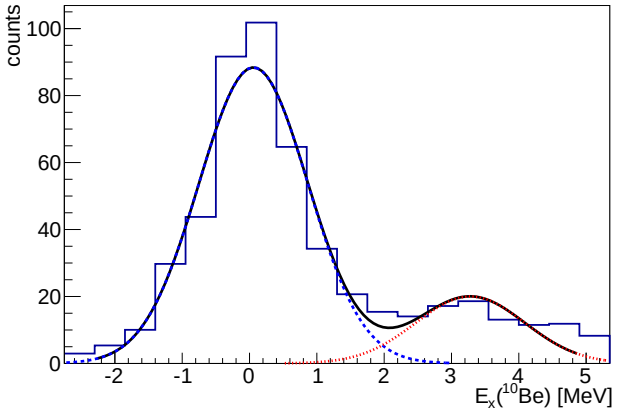

Fig. 3. ^{10}Be excitation spectrum after applying the triple-coincidence cut and after background substraction. The ground state and the first excited state are simultaneuosly fit with two Gaussians (full line). The parameters extracted from the fit are used to separately plot the two Gaussians, for the ground state (dashed line) and the first excited state (dotted line).

$$E_x = \sqrt{(M_{^{12}C} + \omega - E_{p_1} - E_{p_2})^2 - (\boldsymbol{q} - \boldsymbol{p}_{p_1} - \boldsymbol{p}_{p_2})^2} - M_{^{10}Be} \quad (6)$$

The background was subtracted as described above and the resulting ^{10}Be excitation spectrum is presented in Figure 3. The ground-state and the first excited state are identified by making a simulataneous double Gaussian fit to the data. The measured width of the ground state ΔE_x = 1.8 MeV (FWHM) is sufficient to separate it from the first excited state state found at $E_x = 3.29 \pm 0.16$ MeV, which is in agreement with the published data [55,56]. The background-to-signal ratio in the selected ground state region was about 1/3.

4.2.4 Cross section extraction

Since the detector set-up covers a finite phase-space accessible by the reaction, the measure of the reaction probability is given by the differential cross-section. For a simple case when it is constant over the covered phase-space volume V_{ph}, it is given by:

$$\frac{d\sigma}{d\Omega} = \frac{N}{\varepsilon \, \mathcal{L} \, V_{ph}} \quad (7)$$

where $\mathcal{L}$ is the integrated luminosity, N the total number of detected events and ε the efficiency. In the unpolarized ^{12}C(e,e′pp)^{10}Be scattering reaction, the differential cross-section is nine-fold, since we have nine independent kinematical variables in the final state. If the detector set-up has sufficient resolution it enables measuring the cross-section variation inside the detector acceptance. In this paper we present the cross-section as a function of the momentum of the recoiling nucleus, p_m.

If the recoiling nucleus is left in a definite final state, e.g. ground state (GS), another kinematical variable - the final state energy, is fixed. Therefore, the differential cross section for the transition to a definite final state becomes eight-fold. It can be expressed as:

$$\frac{d^8\sigma}{d\Omega_{e'} dE' d\Omega_{p_1} dT_{p_1} d\Omega_{p_2}}(p_m) = \frac{N_{GS}(p_m)}{\epsilon \mathcal{L} < V^8_{ph}(p_m) >} \quad (8)$$

where $N_{GS}(p_m)$ is the background-corrected number of events in the ground state of ^{10}Be, ϵ is the detector efficiency and $\mathcal{L}$ is the integrated luminosity. E' and T_{p1} are kinetic energies of the outgoing electron and the forward ejected proton, respectively. The factor $< V^8_{ph}(p_m) >$ is the phase-space covered by the detectors for a given bin of p_m. The N_{GS}, ε and $\mathcal{L}$ are experimentally measured. The phase-space volume cannot be calculated analytically, therefore we used a Monte-Carlo simulation.

4.2.5 Phase-Space Simulation

The Monte Carlo simulation [57] generates the two ejected protons isotropically in their respective detector acceptances and then calculates the phase-space accessible to the scattered electron based on the energy and momentum conservation, the known beam energy, target mass, mass of the recoiling nucleus and its final state (i.e. the ground-state).

The phase-space as a function of the momentum of the recoiling nucleus, p_m, is then given by:

$$< V^8_{ph}(p_m) > = \frac{N_{bin}(p_m)}{N_{tot}(p_m)} \Lambda \quad (9)$$
$$\text{with } \Lambda = \Delta\Omega_{e'} \Delta E' \Delta\Omega_{p_1} \Delta T_{p_1} \Delta\Omega_{p_2}$$

where $N_{bin}(p_m)$ is the simulated number of events with a given bin of p_m, $N_{tot}(p_m)$ is the total simulated number of events and Λ is the experimental acceptance of the detector set-up. The simulation smears the generated observables with realistic detector resolutions. The particle energy losses inside the target were simulated as well, including radiative corrections.

Table 1. The contributions of the systematic errors to the cross section.

Source of error	Contribution
Phase space simulation	8.8 %
Luminosity calculation	5.2 %
Background subtraction	1.9 %
Detector efficiency	1.7 %
Ground state cut	0.8 %
Total systematic error	10.6 %

4.2.6 Error estimation

The errors of the measured cross section have statistical and systematic sources. The statistical errors are related to the number of events in each bin of the measured observable before background subtraction.

The largest contribution comes from the uncertainty of the phase-space simulation, due to the difference in the shape of the ground state peak in simulation and data. The second largest contribution comes from the error of the luminosity calculation caused by the uncertainty of the target angle with respect to the beam. The third contribution comes from the uncertainty of the background estimation, due to inhomogenities of the background shape. The uncertainty of the combined detector efficiency is another contribution and another comes from the cut on the ground state of ^{10}Be, which can potentially have a small contribution from the first excited state. This contibution is estimated from the Gaussian fits in the Figure 3.

5 Results and Discussion

The differential cross section for the ^{12}C(e,e′pp)^{10}Be$_{g.s.}$ reaction has been extracted as a function of the momentum of the recoiling nucleus, $p_m = |\boldsymbol{p_m}|$. In super-parallel kinematics this momentum is either parallel or anti-parallel to the momentum transfer $\boldsymbol{q}$, so we define p_m to be positive when parallel and negative when anti-parallel to $\boldsymbol{q}$. The events in the ^{10}Be ground state have been selected by applying a cut on the excitation energy $|E_x| \leq 1.8$ MeV.

The acceptances of the detectors determine the range of p_m between -90 MeV/c and 120 MeV/c for which the differential cross section was determined. It was calculated according the relation (8) with a bin width for p_m of 30 MeV/c and the final values are reported in Table 2 and Figure 4.

The differential cross sections calculated with the two different approaches for the two-nucleon overlap, described in Sec. 2, are also shown in Fig. 4. The two results are dramatically different. The dashed line corresponds to the overlap of Eq. (4), where only SRC are included by means of a central and state-independent correlation function. This simpler model is unable to describe the size and the shape of the experimental cross section, which is underestimated by about one order of magnitude. A larger cross section and a much better description of data is given by the full line corresponding to the microscopic calculation based on the SCGF method. The main cause for the enhancement of the cross section is low energy correlations between the two protons, which are taken into account in the two-nucleon DRPA through the fragmentation of the single particle spectral function and the in-medium scattering of the two nucleons. These LRC effects interfere constructively with SRC contributions, increasing the reactions rate by an order of magnitude and reproducing the observed dependence on p_m. The resulting microscopic calculation is found in fairly good agreement with the experimental cross section.

Table 2. The differential cross section of the ^{12}C(e,e′pp)^{10}Be$_{g.s.}$ reaction. The values refer to bin centers of p_m with the bin width of 30 MeV/c.

p_m [MeV/c]	$\frac{d^8\sigma}{d\Omega_{e'}dE'd\Omega_{p_1}dT_{p_1}d\Omega_{p_2}}$ [$10^{-6} fm^4 sr^{-3}$]
-75.0	1.8 ± 0.3 (stat) ± 0.2 (sys)
-45.0	2.4 ± 0.2 (stat) ± 0.2 (sys)
-15.0	3.4 ± 0.4 (stat) ± 0.4 (sys)
15.0	2.6 ± 0.4 (stat) ± 0.3 (sys)
45.0	1.8 ± 0.2 (stat) ± 0.2 (sys)
75.0	1.2 ± 0.1 (stat) ± 0.1 (sys)
105.0	0.3 ± 0.2 (stat) ± 0.03 (sys)

In the (uncorrelated) independent particle model, the recoiling momentum $\boldsymbol{p_m}$ yields the total momentum of the struck pp pair. Hence, the measured cross section suggests that two-proton substructures in the ^{12}C target carry a rather uniform total momentum up to about 100 MeV/c but with zero momentum states being more probable. Note that the two-nucleon overlap function depends only on the magnitude of the recoiling momentum, p_m, due to spherical symmetry. Hence, the asymmetries in the measured and calculated cross sections of Fig. 4 are due to nuclear currents and FSI effects. Measurements in different kinematics, with $\boldsymbol{p_m}$ not aligned with the momentum transfer $\boldsymbol{q}$, may bring useful information not only to test the structure of this nucleus and NN correlations but also to better understand and improve our reaction theories for the two-body currents and FSI.

In conclusion, we have measured the exclusive reaction ^{12}C(e,e′pp)^{10}Be$_{g.s.}$ and separated for the first time the ground state of the recoiling nucleus. A silicon detector telescope and two high-resolution spectrometers were used to detect the scattered electron and the two emitted protons. These allowed for a clean separation of the ^{10}Be ground state and to extract the eight-fold differential cross section with high precision. Theoretical calculations based on the SCGF method for the structure part and the Pavia model for the scattering mechanism are able to describe the experimental data. The calculated cross sections are very sensitive to the treatment of correlations in the two-nucleon overlap. These results suggest that in the present kinematics and with the present choice of the Bonn-C nuclear interaction, that contains a short-range repulsive core, the cross section is dominated by a strong interplay between SRC and LRC of proton pairs from the $p_{3/2}$ orbits.

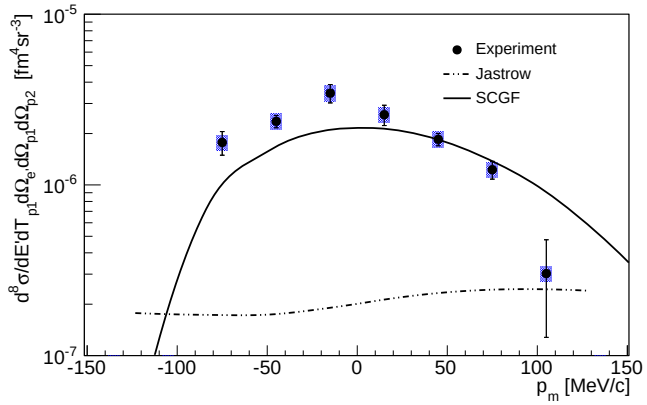

Fig. 4. The differential cross section of the ^{12}C(e,e′pp)^{10}Be$_{g.s.}$ reaction as a function of the momentum of the recoiling nucleus, p_m. The vertical straight lines behind the experimental points represent the statistical errors, while the shaded bars are the systematic errors. The dash-double-dotted line gives the cross section calculated with the overlap function of Eq. (4), while the full line is the result from SCGF in the two-hole DRPA, which includes all correlations microscopically.

This work was supported in part by the Deutsche Forschungsgemeinschaft with the Collaborative Research Centers 443 and 1044, by the Croatian Science Foundation under project HRZZ 1680 and Technology Facilities Council (STFC) under grant No. ST/L005743/1.

References

1. V. Pandharipande *et al.*, Rev. Mod. Phys. **69**, 981 (1997).
2. W. H. Dickhoff, C. Barbieri, Prog. Part. Nucl. Phys. **52**, 377 (2004).
3. R. Jastrow, Phys. Rev. **81**, 165 (1951).
4. R. Schiavilla *et. al.*, Phys. Rev. Lett. **98**, 132501 (2007).
5. R. Subedi *et al.*, Science **320**, 1476 (2008).
6. S. Boffi, C. Giusti, F.D. Pacati and M. Radici *Electromagnetic Response of Atomic Nuclei* (Claredon Press, Oxford 1996).
7. J. J. Kelly, Adv. Nucl. Phys. **23**, 75 (1996).
8. L. Lapikas, Nucl. Phys. A **553**, 297c (1993).
9. C. Barbieri, Phys. Rev. Lett. **103**, 202502 (2009).
10. A. Cipollone *et. al.*, Phys. Rev. C **92**, 014306 (2015).
11. I. Bobeldijk *et al.*, Phys. Rev. Lett. **73** 2684 (1994).
12. P. Monaghan *et al.*, J. Phys. G: Nucl. Part. Phys. **41**, 105109 (2014).
13. K. Hebeler *et. al.*, Ann. Rev. Nucl. Part. Sci. **65**, 457 (2015).
14. A. Carbone *et. al.*, Phys. Rev. C **90**, 054322 (2014).
15. A. Ekström *et. al.*, Phys. Rev. C **91**, 051301(R) (2015).
16. D. Rohe *et al.*, Phys. Rev. Lett. **93**, 182501 (2004).
17. C. Barbieri and L. Lapikás, Phys. Rev. C **70**, 054612 (2014).
18. C. Barbieri, Nuclear Physics B **159**, 174 (2006).
19. R. Shneor *et al.*, Phys. Rev. Lett. **99**, 072501 (2007).
20. E. Piasetzky *et al.*, Phys. Rev. Lett. **97**, 162504 (2006).
21. I. Korover *et. al.*, Phys. Rev. Lett. **113**, 022501 (2014).
22. O. Hen *et. al.*, Science **346**, 614 (2014).
23. K. Gottfried, Nucl. Phys. **5**, 557 (1958).
24. D. L. Groep *et al.*, Phys. Rev. C **63**, 014005 (2000).
25. C. Giusti *et al.*, Phys. Rev. C **57**, 1691 (1998).
26. H. Müther and A. Polls, Prog. Part. Nucl. Phys. **45**, 243 (2000).
27. C. Barbieri *et al.*, Phys. Rev. C **70**, 014606 (2004).
28. C.J.G. Onderwater *et al.*, Phys. Rev. Lett. **78**, 4893 (1997).
29. C.J.G. Onderwater *et al.*, Phys. Rev. Lett. **81**, 2213 (1998).
30. R. Starink *et al.*, Phys. Lett. B **474**, 33 (2000).
31. G. Rosner, Prog. Part. Nucl. Phys. **44**, 99 (2000).
32. A. Zondervan *et al.*, Nucl. Phys. A **587**, 697 (1995).
33. L. J. H. M. Kester *et al.*, Phys. Rev. Lett. **74**, 1712 (1995).
34. K. I. Blomqvist *et al.*, Nucl. Phys. A **626**, 871 (1997).
35. M. Makek *et al.*, Nucl. Instr. Meth. in Phys. Res. A **673**, 82 (2012).
36. K. I. Blomqvist *et al.*, Nucl. Instr. Meth. in Phys. Res. A **403**, 263 (1998).
37. C. Giusti, F.D. Pacati, Nucl. Phys. A **615**, 373 (1997).
38. C. Giusti *et al.*, Eur. Phys. J. A **26**, 209 (2005).
39. C. Giusti, F.D. Pacati, Nucl. Phys. A **641**, 297 (1998).
40. P. Wilhelm *et al.*, Z. Phys. A **359**, 467 (1997).
41. C.C. Gearhart, Ph.D. thesis, Washington University, St. Louis (1994); C.C. Gearhart, W.D. Dickhoff, private communication.
42. C. Barbieri and M. Hjorth-Jensen, Phys. Rev. C **79**, 064313 (2009).
43. C. Barbieri and W. H. Dickhoff, Phys. Rev. C **65**, 064313 (2002).
44. R. Machleidt, Adv. Nucl. Phys. **19**, 191 (1989)
45. H. Mu?ther *et al.*, Phys. Rev. C **51**, 3040 (1995).
46. D. Van Neck *et al.*, Phys. Rev. C **57**, 2308 (1998).
47. D. Middleton *et al.*, Eur. Phys. J. A **29**, 261 (2006).
48. D. Middleton *et al.*, Eur. Phys. J. A **43**, 137 (2010).
49. A. Nadasen *et al.*, Phys. Rev. C **23**, 1023 (1981).
50. M. Schwamb *et al.*, Eur. Phys. J. A **17**, 7 (2003).
51. M. Schwamb *et al.*, Eur. Phys. J. A **20**, 233 (2004).
52. C. Giusti, F. Pacati, and M. Schwamb, *Proceedings of the XVII International School on Nuclear Physics, Neutron Physics and Nuclear Energy* (Varna 2007), BgNS Transactions, v.5, No.1, p.56-67 (2009), arXiv:0801.2304v1 (2008).
53. C. Giusti *et al.*, Eur. Phys. J. A **31**, 155 (2007).
54. C. Giusti *et al.*, Eur. Phys. J. A **33**, 29 (2007).
55. D.R. Tilley *et al.* Nucl. Phys. A745 155 (2004)
56. N. I. Ashwood *et al.*, Phys. Rev. C **68**, 017603 (2003).
57. M. Distler *et al.*, in *Proceedings of the 12th IEEE real time congress on nuclear and plasma sciences* (E. Schanciz, 2001).